

1 **Seasonal freeze-thaw cycles and permafrost degradation**  
2 **on Mt. Zugspitze (German/Austrian Alps) revealed by**  
3 **single-station seismic monitoring**

4 **Fabian Lindner<sup>1</sup>, Joachim Wassermann<sup>1</sup>, Heiner Igel<sup>1</sup>**

5 <sup>1</sup>Department of Earth and Environmental Sciences, LMU Munich, Theresienstraße 41, 80333, Munich,  
6 Germany

7 **Key Points:**

- 8 • We use a single seismic station deployed near a permafrost body on Mt. Zugspitze  
9 (Germany) to monitor freeze-thaw processes over 15 years  
10 • Cross-correlations between the sensor components reveal seasonal velocity change  
11 cycles and a long-term velocity decrease  
12 • The changes are due to seasonal freeze-thaw cycles and permafrost degradation,  
13 suggesting seismology as effective permafrost monitoring tool

---

Corresponding author: F. Lindner, [flindner@geophysik.uni-muenchen.de](mailto:flindner@geophysik.uni-muenchen.de)

**Abstract**

Thawing of mountain permafrost in response to rising temperatures degrades the stability of rock walls and thereby affects infrastructure integrity in Alpine terrain. In this study, we use 15 years of passive seismic data from a single station deployed near a known permafrost body on Mt. Zugspitze (Germany), to monitor freeze-thaw processes. The recordings reveal a persistent cultural seismic noise source, which we utilize to compute single-station cross-correlations and extract relative seismic velocity changes. We find that parts of the cross-correlations show seasonal velocity variations ( $\approx 3\%$  peak-to-peak amplitude) and a long-term velocity decrease ( $\approx 0.1\%/yr$ ). Comparison with meteorological data and a previous electrical resistivity tomography study suggests that these velocity changes are caused by active-layer freeze-thaw cycles and by permafrost degradation, respectively. The results demonstrate the potential of passive seismology for permafrost monitoring and suggest that denser instrumentation will provide detailed spatio-temporal insights on permafrost dynamics in future studies.

**Plain Language Summary**

Climate change causes permafrost (year-round frozen rock) warming and thawing, which destabilizes rock slopes and thus constitutes a hazard potential. However, unlike glacier retreat, permafrost thawing cannot be directly observed from the surface and requires special imaging techniques for monitoring. Here, we use seismic waves generated by cable cars and other man-made infrastructure to probe permafrost on Mt. Zugspitze (Germany) and track temporal changes over the past 15 years. Results from a single seismic station show that the seismic wave propagation velocity in the rock is subject to seasonal variations (difference between late winter and late summer of up to 3%) and a long-term decrease of roughly 0.1% per year. As the seismic velocity is generally higher in frozen rock compared to unfrozen rock, the seasonal changes can be well explained by seasonal thaw and refreeze, and the long-term changes by ongoing permafrost thawing. Because passive seismology is labour and cost effective compared to common techniques requiring active signal excitation, seismology constitutes a promising new approach for continuous long-term permafrost monitoring.

**1 Introduction**

Permafrost refers to the perennially frozen ground and underlies more than 20% of the Northern Hemisphere land area (Zhang et al., 2008) including high-elevation areas in the European Alps. With rising atmospheric temperatures, permafrost warming and thawing are observed (Beniston et al., 2018; Biskaborn et al., 2019; Mollaret et al., 2019), which affects the rock mechanical properties and degrades the stability of slopes (Davies et al., 2001; Mellor, 1973; Haerberli et al., 2010; Krautblatter et al., 2013). As a consequence, climate change is expected to result in an increase in rock detachments in permafrost areas (Gruber & Haerberli, 2007), already observable by a correlation between rockfall activity and temperatures (Raveland et al., 2017; Huggel et al., 2012; Gruber et al., 2004a). In addition, individual larger, partly catastrophic rock detachments from permafrost affected mountains have been documented in recent years (Walter et al., 2020; Phillips et al., 2017; Pirulli, 2009). This highlights the hazard potential of permafrost degradation for infrastructure and settlements, and thus the importance to understand and monitor the spatio-temporal evolution of mountain permafrost.

The occurrence of permafrost can be delineated to areas with long-term mean annual air temperatures below the freezing point, with colder temperatures favoring larger volumes of permafrost (Haerberli et al., 2010). Yet, the site specific permafrost conditions are affected by topography (Noetzli & Gruber, 2009), the local solar radiation conditions (Hoelzle et al., 2001), and the exposure to the atmosphere. Steep rock walls are usually free of debris, which promotes a rapid response to changes in the thermal forcing (Gruber

et al., 2004b), whereas debris and snow cover have an insulating effect. In addition to the thermal forcing through heat conduction, advective heat transfer through (melt)water percolation can rapidly develop deep thaw corridors in fractured rocks (Kane et al., 2001). The complex interplay between numerous processes results in a heterogeneous three-dimensional distribution of mountain permafrost in lenses rather than layers (Krautblatter & Hauck, 2007).

Permafrost bodies can be monitored directly through temperature logging in boreholes (Haeberli et al., 1998; Beniston et al., 2018) or through surface-based geophysical imaging techniques including electrical resistivity tomography (ERT) and active seismics (Kneisel et al., 2008; Hauck, 2013). These methods can be used to differentiate between frozen and unfrozen ground (Hauck, 2002; Timur, 1968; King, 1977; Harris & Cook, 1986; Kneisel et al., 2008), or to even infer the temperature distribution in the case of ERT (Krautblatter et al., 2010; Scandroglio, Draebing, et al., 2021). While boreholes allow continuous permafrost monitoring, their wider applicability is limited by the logistics and costs involved. In contrast, active geophysical imaging techniques offer more flexibility but must be applied repeatedly to obtain temporal resolution. This remains challenging, as automatic acquisition in harsh Alpine terrain is difficult and manual acquisition e.g. on a monthly basis (Mollaret et al., 2019) is laborious.

To circumvent these limitations, passive seismic methods have been recently explored for permafrost monitoring. Applying ambient-noise based seismic interferometry, i.e. extracting repeatedly the seismic impulse response between pairs of seismic stations, James et al. (2019) find seasonal velocity changes of a few percent over the course of two years at a permafrost site in Alaska, which they attribute to active-layer freeze-thaw cycles. Using an array of continuously recording sensors, James et al. (2019) gain both spatial insights on the thaw depth and high temporal resolution such that they can track permafrost thawing caused by water infiltration from snow melt and rainfall events. Similar results are reported by Guillemot et al. (2020), who find seasonal changes in seismic velocities related to permafrost dynamics in the upper 10 m of a rock glacier. In this study, we investigate the potential of single-station passive seismology for continuous long-term permafrost monitoring. For this purpose, we apply seismic interferometry to a station deployed on the ridge of Mt. Zugspitze (Germany) close to a known permafrost lens. Data are available for the past 15 years and we extract seismic velocity change time series, which we compare to meteorological records and a previous ERT study.

## 2 Study site and seismic data

### 2.1 Mt. Zugspitze

Located at the German-Austrian border, Mt. Zugspitze (2962 m asl, WGS84 coordinates of the summit: 47.42119, 10.98634) is the highest peak in Germany. The summit area hosts three cable car stations and various other infrastructure including restaurants and broadcasting facilities (Fig. 1). Mt. Zugspitze is composed of triassic limestone (Wettersteinkalk) being weathered and fractured in the summit area and characterized by a subsurface cave drainage system established by Karst dissolution (Gude & Barsch, 2005; Krautblatter et al., 2010). Excavations for cable cars and other constructions revealed that the fractures are filled with up to decameter thick ice lenses and frozen loam (Körner & Ulrich, 1965; Ulrich & King, 1993). In prehistoric times, around 3700 years before present, a giant 0.3–0.4 km<sup>3</sup> rock slide occurred from the summit region, which is considered to have been triggered by permafrost degradation at the end of the Holocene climatic optimum (Jerz & von Poschinger, 1995).

In present times, permafrost is found in the north-facing rock, whereas the south-facing slopes are almost free of permafrost (Gude & Barsch, 2005; Nötzli et al., 2010). In 2007, a borehole was drilled beneath the summit, intersecting the crest entirely from

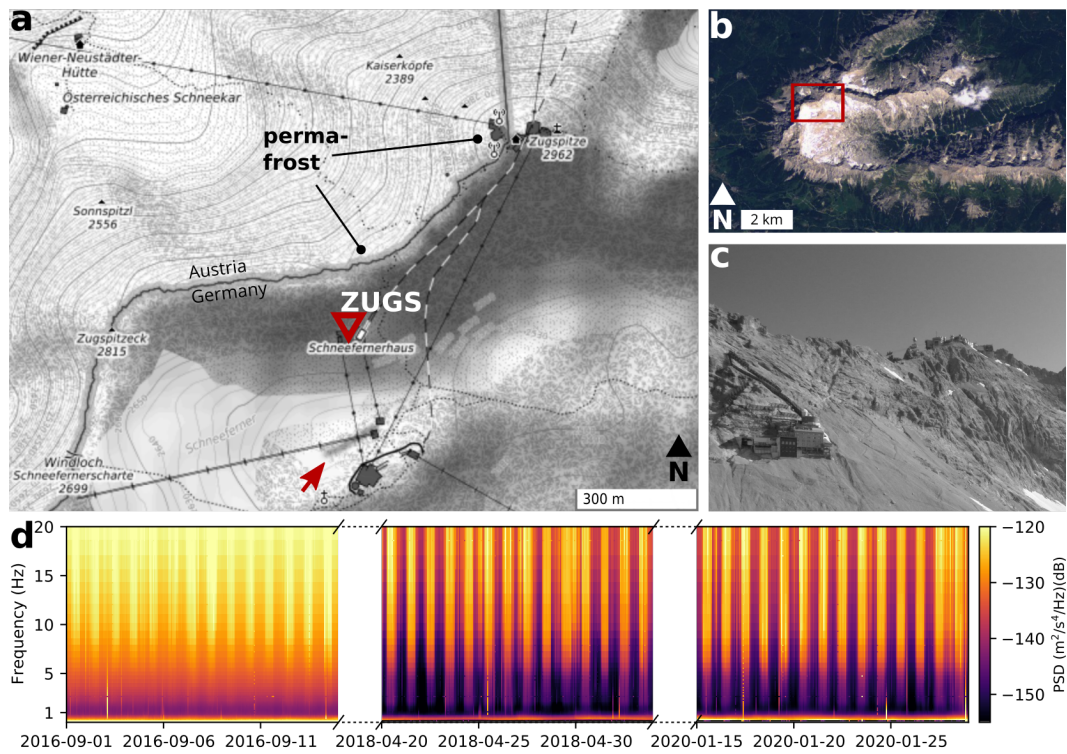


**Figure 1.** (a) Topographic map of the Zugspitze with the location of the the seismic station BW.ZUGS (red triangle) and two known permafrost areas. Black dotted lines are cable cars, black-white dashed lines are railway tunnels (map: OpenTopoMap). (b) Western part of the Wetterstein mountain range, the red rectangle shows the map extent from (a) (picture: Sentinel, 2017-06-26). (c) Photo of the permafrost affected ridge with the Schneefernerhaus (left) and the Zugspitze summit (right). View perspective is indicated by the red arrow in (a). (d) Vertical component spectrograms of station BW.ZUGS for two weeks in September 2016, April to May 2018, and January 2020 showing a persistent noise source during daytimes.

114 south to north on a length of 44 m. Temperature logging inside the borehole reveals per-  
 115 mafrost temperatures down to about  $-4^{\circ}\text{C}$  and seasonal thaw depths of 4.5 m and 1.5 m  
 116 from the southern and northern side, respectively (Nötzli et al., 2010; Gallemann et al.,  
 117 2017). Another permafrost body extends several tens of meters along the ridge north of  
 118 the Schneefernerhaus research station (Fig. 1b) (Krautblatter et al., 2010), which is ev-  
 119 ident by perennial ice in a gallery intersecting the ridge. While the mean annual air tem-  
 120 perature measured at the summit between 1901 and 2000 was  $-4.8^{\circ}\text{C}$ , it was  $-3.7^{\circ}\text{C}$  be-  
 121 tween 2001 and 2020, hence more than  $1^{\circ}\text{C}$  higher compared to the twentieth century.  
 122 The increasing temperatures are reflected by permafrost warming and degradation vis-  
 123 ible in the borehole temperature logs beneath the summit (Gallemann et al., 2017).

## 124 2.2 Instrumentation

125 The Schneefernerhaus accommodates the permanent seismic station BW.ZUGS (Department  
 126 of Earth and Environmental Sciences, Geophysical Observatory, LMU Munich, 2001) in  
 127 a vault next to the rock face, which is operational since 2006 (Fig. 1). Initially, the sta-  
 128 tion was equipped with a Mark L4-3D short-period seismometer (natural frequency of  
 129 1 Hz) and a Lennartz M24 digitizer. In August 2017, this setup was replaced by a Gu-  
 130 ralp CMG-3T broadband sensor and a Reftek RT130 digitizer. After a larger data gap  
 131 starting in May 2018, the Guralp sensor was replaced by a Trillium Compact 120 s sei-  
 132 smometer, which is operational since July 2019. The ground velocity output of all three  
 133 sensors is sampled at 200 Hz. Spectrograms for the three different sensors at different  
 134 times of the year (Fig. 1d) reveal a noise source being persistent over years with strong  
 135 ground vibrations during the day, bound by the operation hours of the cable cars. De-  
 136 spite lower amplitudes at lower frequencies, the noise source is visible down to 2 Hz, where  
 137 amplitudes are close to the self-noise level of the Mark L4-3D seismometer. Temporary  
 138 deployments of two additional stations in February 2019 show that the noise amplitudes  
 139 are stronger for installations closer to the summit area (not shown), suggesting the lat-  
 140 ter as excitation area.

## 141 3 Single-station monitoring and data processing

142 We utilize the single station to compute cross-correlations between the different sen-  
 143 sor components (E, N, Z resulting in EN, EZ, NZ cross-correlations), which can be con-  
 144 sidered as impulse response retrieval for a source and a receiver being colocated (Hobiger  
 145 et al., 2014; De Plaen et al., 2016; Yates et al., 2019). The single-station cross-correlations  
 146 contain scattered and reflected waves with the EN component being sensitive to Rayleigh  
 147 and Love waves, whereas the EZ and NZ components relying on vertical ground motions  
 148 are not sensitive to Love waves. In addition to surface waves, the cross-correlations may  
 149 also contain body waves reflected at depth including P-to S- and S-to P-converted phases  
 150 (Hobiger et al., 2014; Becker & Knappmeyer-Endrun, 2019). We use the MSNoise pack-  
 151 age (Lecocq et al., 2014) to compute daily cross-correlations, which we form by stack-  
 152 ing individual cross-correlations calculated from non-overlapping 30-minute windows and  
 153 the frequency range of 0.1 to 25 Hz. The preprocessing includes the removal of the in-  
 154 strument response from the raw data, clipping of the seismograms at three times the root  
 155 mean square amplitude, and spectral whitening to equalize the amplitude of all frequen-  
 156 cies (Bensen et al., 2007) (all MSNoise processing parameters are provided in Table S1).  
 157 Spectral whitening increases the robustness of the cross-correlations against noise source  
 158 variability but cannot be applied for auto-correlations of individual channels as this re-  
 159 sults in a perfect delta pulse not carrying any information on the medium. The inhib-  
 160 ited applicability of spectral whitening is the main disadvantage of auto-correlations (Hobiger  
 161 et al., 2014). This is confirmed by this study, where the auto-correlation results appear  
 162 to be similar to the single-station cross-correlations results, but noisier. We therefore fo-  
 163 cus on the single-station cross-correlations in this work.

164 To extract seismic velocity changes expressed as travel time changes, we compare  
 165 the time-lapse cross-correlations against a reference cross-correlation. One common ap-  
 166 proach for this purpose is the moving-window cross-spectral (MWCS) technique (Clarke  
 167 et al., 2011), where one employs a sliding window along the coda of bandpass filtered cross-  
 168 correlations. The sliding window is used to determine the travel time shift  $\delta t$  as a func-  
 169 tion of the lag time  $t$ , averaged over the width of the sliding window and the frequency  
 170 range of consideration. In a second step, one determines the slope  $-\delta t/t$  through a lin-  
 171 ear regression, which is equal to the velocity change  $dv/v$  relative to the reference, if the  
 172 latter affects the subsurface uniformly. Being related to the MWCS technique, we here  
 173 explore the recently introduced wavelet cross-spectrum method (Mao et al., 2020), which  
 174 also yields travel time shifts relative to the reference cross-correlation, but as a function  
 175 of lag time and frequency  $f$ , i.e.  $\delta t(t, f)$ , hence with increased joint time-frequency res-  
 176 olution. This enables us to investigate specific parts of the cross-correlation. Here, we  
 177 use the wavelet cross-spectrum implementation of the NoisePy package (Jiang & Denolle,  
 178 2020), employing a Morlet wavelet to compare 15 d cross-correlation stacks (calculated  
 179 in a moving window with a step size of one day) against the reference. Regarding the  
 180 reference, we consider two approaches. (1) We calculate the linear reference stack for the  
 181 fixed reference period of 2017-09-01 to 2018-05-01 using all available daily cross-correlations.  
 182 (2) As the seasonal freeze-thaw cycle associated with permafrost can cause such strong  
 183 velocity changes relative to a fixed reference that the measurement of travel time shifts  
 184 is affected by cycle skipping (James et al., 2017, 2019), we also consider a moving-reference  
 185 type approach to mitigate this problem. To this end, we use 2016 as reference year, where  
 186 we determine the seasonal travel time variations from adjacent 15 d stacks. Subsequently,  
 187 for all other times, we determine the travel time variations as those of 2016 plus devi-  
 188 ations to 2016 (e.g.  $\delta t_{2017-03-17} = \delta t_{2016-03-17} + \delta t_{2017-03-17vs2016-03-17}$ , see Text S1 for  
 189 details).

## 190 4 Results

191 Active layer thaw and refreeze are governed by the temperature signal propagat-  
 192 ing into the rock with a period of one year. If cross-correlation coda waves sample freeze-  
 193 thaw areas, we expect a periodic velocity change signal with the same period. We thus  
 194 calculate the amplitude of the 365.25 d periodicity,  $A_{LS}(365.25 d)$ , of all  $\delta t$  time series  
 195 obtained from the wavelet cross-spectrum method relative to the fixed reference in the  
 196 lag time of -5 s to 5 s and frequency range of 1 Hz to 20 Hz. Because Fourier analysis  
 197 is hindered by data gaps in the  $\delta t$  time series, we employ the Lomb-Scargle periodogram  
 198 (Lomb, 1976; Scargle, 1982), which enables us to compute power spectra at specific fre-  
 199 quencies independent of the sample spacing. Fig. 2a-c shows  $A_{LS}(365.25 d)$  as a func-  
 200 tion of lag time and frequency, revealing that parts of the cross-correlations exhibit sea-  
 201 sonal changes with a period of one year. This is further emphasized by the three  $\delta t$  time  
 202 series (converted to  $-\delta t/t$ ) representing specific lag-frequency combinations showing clear  
 203 seasonal variations (Fig. 2d). Complementary to the individual  $-\delta t/t$  curves, Fig. 2d also  
 204 depicts the lag and frequency dependent  $-\delta t/t$  measurements limits (horizontal dashed  
 205 lines), beyond which cycle skipping occurs. While the two lower considered frequencies  
 206 stay within these limits, the higher frequency  $-\delta t/t$  curve (EZ, 9.92 Hz) is affected by  
 207 cycle skipping as the variations are larger than the measurement limits.

208 To systematically investigate temporal changes, we consider the frequency depen-  
 209 dence of  $-\delta t/t$ . Because we expect localized changes rather than uniform changes, we  
 210 refrain from determining  $-\delta t/t$  via linear regression, and instead determine the median  
 211 from individual  $-\delta t/t$  curves for each frequency bin. We restrict our analysis to the lag  
 212 range bound by one and 15 times the respective period on the positive and negative branch  
 213 of the cross-correlations (white dashed lines in Fig. 2a-c), hence using the same number  
 214 of cycles independent of frequency. In addition, we only consider individual  $-\delta t/t$  time  
 215 series associated with a normalized Lomb-Scargle amplitude of at least 0.15, i.e.  $A_{LS}(365.25 d) \geq$

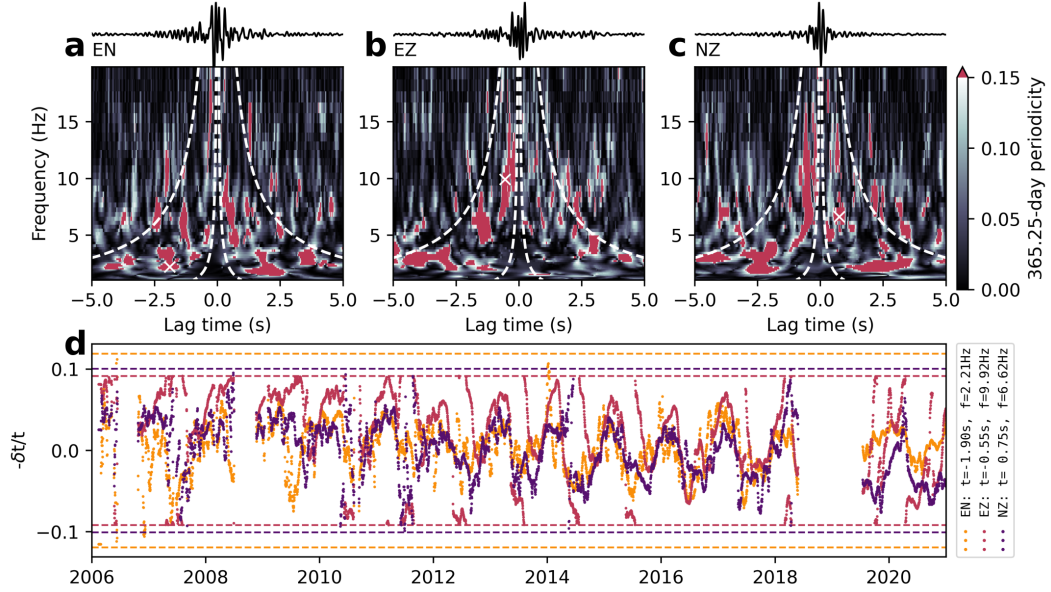


**Figure 2.** (a)-(c) EN, EZ, and NZ component cross-correlation reference stacks (seismograms, bandpass filtered 2-8 Hz) and 365.25 d periodicity of travel time shifts relative to the fixed reference (color maps). Red spots indicate combinations of lag time and frequency in the cross-correlations (joint time-frequency resolution achieved through wavelet-based cross-spectra) with a significant one-year period signal. White dashed lines indicate the frequency dependent lag times of one and 15 periods. (d) Travel time shifts (converted to  $-\delta t/t$ ), for a lag-frequency combination of each component with high 365.25 d periodicity (white crosses in (a)-(c)). The horizontal dashed lines indicate the maximum  $-\delta t/t$  measurement ranges for the three curves, outside of which cycle skipping occurs.

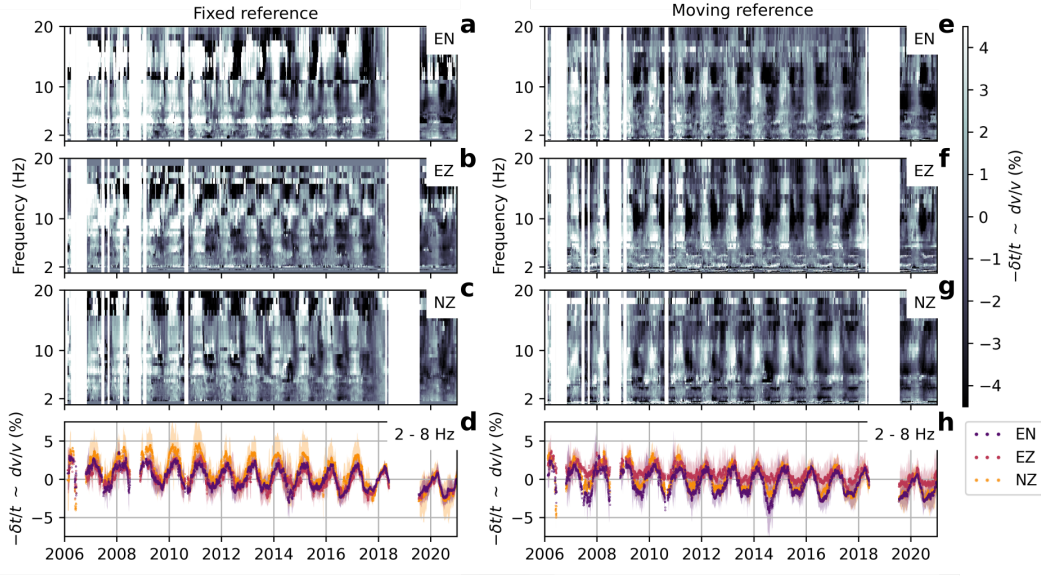


**Figure 3.** (a)-(c) Median travel time change  $-\delta t/t$  for each frequency bin, computed from all individual time series associated with high 365.25 d periodicity ( $A_{LS} \geq 0.15$ ) in the lag range bound by one and 15 periods. Results for all three components are relative to the fixed reference. (d) Average  $-\delta t/t$  over the frequency range 2-8 Hz (dotted lines) with one standard deviation (shaded areas). (e)-(h) Same as (a)-(d) for the moving reference approach.

0.15 (Fig. 2a-c), to focus on coda waves that are subject to seasonal variations. Fig. 3a-c shows that the seasonal pattern is most consistent for the lower frequencies, whereas above about 8 Hz, especially component EZ shows a different behaviour. Taking the average over the frequency range of 2-8 Hz (Fig. 3d) reveals a similar pattern for all three components with high velocities (high values in  $-\delta t/t$ ) in the winter months and low velocities in the summer months. In addition, the time series exhibit a long-term velocity decrease.

To investigate potential artifacts due to cycle skipping when using the fixed reference, Fig. 3e-h shows the results for the moving reference approach (same processing otherwise). In this case, the seasonal pattern emerges more consistently over a broader frequency range, extending beyond 10 Hz. However, the 2-8 Hz averaged  $-\delta t/t$  curves are similar as those for the fixed reference. While in the latter case, component EN is associated with an increased standard deviation (purple shading in Fig. 3d), using the moving reference results in increased uncertainty in component EZ. Regardless of the reference choice, the curves show the same characteristics, i.e. high (low) velocities in winter (summer) months and a long-term velocity decrease. However, careful inspection of Fig. 3e-g also reveals some high-velocity notches in summer, best visible on component EZ in 2011, 2012, 2013, and 2015 above 10 Hz. These features are also visible in Fig. 2d, where component EZ shows summer drops in  $-\delta t/t$  that overshoot the lower cycle skipping limit and subsequently enter the plot again as steep lines from the upper cycle skipping limit. As using the moving reference (in 2016) does not eliminate this type of cycle skipping suggests that some years exhibit changes relative to 2016 that exceed the cycle skipping limit.

## 239 5 Discussion

### 240 5.1 Velocity changes

241 In most seismic monitoring applications,  $-\delta t/t$  is obtained from linear regression  
 242 assuming a bulk velocity change. Here, we find that only parts of the coda waves at dif-  
 243 ferent lag times show clear seasonal changes (Fig. 2a-c), which suggests localized changes  
 244 and we consequently consider  $-\delta t/t$  as a proxy for  $dv/v$ . To attach numbers to the sea-  
 245 sonal and long-term changes, we fit a velocity change model consisting of the superpo-  
 246 sition of a sinusoid with a period of 365.25 d and a linear trend to the  $-\delta t/t$  time series  
 247 (eq (1), supporting information). Using the 2-8 Hz curves and averaging over the three  
 248 components yields seasonal peak-to-peak velocity changes of 3.3% for the fixed reference  
 249 and 2.9% for the moving reference and long-term velocity decreases of -0.14%/yr and -  
 250 0.11%/yr, respectively. In addition to different reference approaches, we further exam-  
 251 ine different strategies in determining  $-\delta t/t$  for component NZ (most consistent com-  
 252 ponent), including linear regression analysis and the classical MWCS technique (see Text S2  
 253 for details). In all cases, we find seasonal velocity changes with high (low) values in late  
 254 winter (summer) and a velocity decrease over the past 15 years. Yet, the amplitudes of  
 255 both characteristics are smaller when using the whole coda wave window independent  
 256 of the 365.25 d periodicity, which further supports that the velocity changes are local-  
 257 ized. The observed 2-8 Hz velocity change characteristics appear to be present also at  
 258 higher frequencies (Fig. 3), however, we refrain from analyzing a frequency dependence,  
 259 as we are facing a complex setting with steep terrain and heterogeneously distributed  
 260 medium changes, which is far off from a layered half space typically assumed e.g. in sur-  
 261 face wave analysis (James et al., 2019). In addition, we encounter cycle skipping at higher  
 262 frequencies, which partly remains even when using a moving reference. This suggests that  
 263 large velocity changes (several percent) between the years are present, which is hardly  
 264 explainable and may therefore also be an artefact of the year-by-year comparison of your  
 265 moving reference approach.

266 The location of the velocity changes can be examined with travel time sensitivity  
 267 kernels for a colocated source and receiver. In this case, the sensitivity kernels for both  
 268 of the two end-member scenarios of single scattering (Pacheco & Snieder, 2006) and mul-  
 269 tiple scattering (Pacheco & Snieder, 2005) peak at the station location and decrease rapidly  
 270 with distance from the station (Bennington et al., 2021; Sens-Schönfelder & Wegler, 2006).  
 271 This implies that the velocity changes relate to the direct surroundings of the station  
 272 (Hobiger et al., 2014) and we hypothesize that they are caused by thaw and refreeze as-  
 273 sociated with the permafrost lens documented in Krautblatter et al. (2010). The per-  
 274 mafrost lens is separated by about 200 m from the station, which is only a fraction of  
 275 one wavelength at the lowest frequencies considered. However, we also note that the sin-  
 276 gular station sensitivity kernels may not comprehensively describe the encountered situ-  
 277 ation with a stationary noise source at the Zugspitze summit in some distance to the sta-  
 278 tion. This situation also admits phases resulting from the cross-correlation of direct waves  
 279 emitted from the noise source and their singly scattered (laterally or at depth) products,  
 280 hence source and receiver being not colocated. This is expected to add travel time sen-  
 281 sitivity also to the noise source region and the direct path between source and receiver  
 282 (both of which are also affected by permafrost), similar as for two-station cross-correlation  
 283 sensitivity kernels (Obermann et al., 2019). To further pinpoint the velocity changes, we  
 284 note however, that denser instrumentation would be necessary.

### 285 5.2 Permafrost dynamics

286 We evaluate our hypothesis of freeze-thaw induced velocity changes by consider-  
 287 ing the recordings from a weather station at the Zugspitze summit run by the Deutscher  
 288 Wetterdienst (DWD, German weather service). Fig. 4 shows the 2-8 Hz velocity changes  
 289 (fixed reference, same as Fig. 3d), as well as the air temperature, snow height and fluid

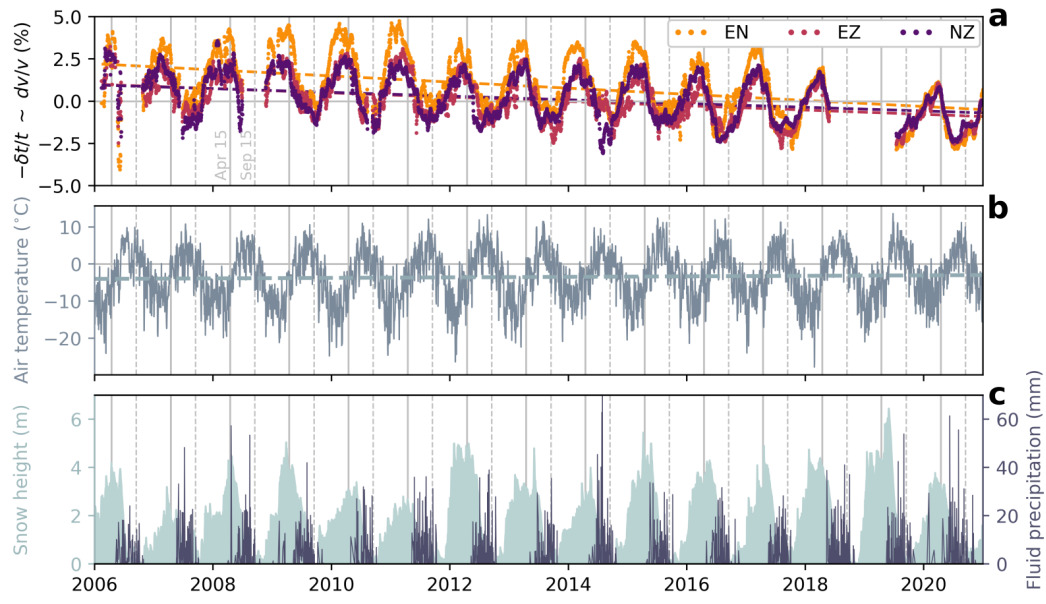


**Figure 4.** (a) 2-8 Hz velocity change (dotted lines, same as in Fig. 3d) and linear trend (dashed lines). Vertical solid and dashed lines indicate April 15 and September 15 of each year. (b) Daily mean air temperature (solid line) with linear trend (dashed line). (c) Snow height (greenish areas) and fluid precipitation (blueish bars). Time series in (b) and (c) are measured at the Zugspitze summit.

290 precipitation measured by the weather station. This reveals that the annual velocity drops  
 291 starting in April (vertical gray solid lines) occur concurrently with air temperatures ris-  
 292 ing above the freezing point. This especially holds when adding an offset of around  $1\text{ }^{\circ}\text{C}$   
 293 to the temperature curve to account for the elevation difference between the summit and  
 294 the ridge (assuming a atmospheric lapse rate of around  $-0.6\text{ }^{\circ}\text{C}/100\text{ m}$ ). Minimum an-  
 295 nual velocities are reached in July and August, followed by a velocity increase starting  
 296 in September, coincidentally with temperatures dropping below the freezing point (ver-  
 297 tical gray dashed lines). With temperatures above the freezing point, the period between  
 298 April and September, where the velocity decreases is furthermore characterized by snow  
 299 melt and rain-dominated precipitation (Fig. 4c). Considering the long-term trend, the  
 300 velocity drops on the order of  $0.1\text{ } \%/ \text{yr}$ , while the temperature rises on average by  $0.07\text{ }^{\circ}\text{C}/\text{yr}$   
 301 in the time period between 2006-01-01 and 2021-01-01. The determined linear trends (us-  
 302 ing eq. (1), supporting information) are depicted by the colored dashed lines in Fig. 4a-  
 303 b.

304 The permafrost lens in the ridge to the north of the seismic station (Fig. 1) is mon-  
 305 itored by time-lapse temperature-calibrated ERT images (Scandroglio, Rehm, et al., 2021;  
 306 Schroeder & Krautblatter, 2021), of which results are documented for 2007 (Krautblatter  
 307 et al., 2010). (Krautblatter et al., 2010) observe pronounced melt from May to August  
 308 with rock temperature changes being too fast to be solely explained by heat conduction.  
 309 Coincidentally, they observe water seepage into the gallery and rapid melting along frac-  
 310 ture zones suggesting warming and melting through water percolation. With temper-  
 311 atures dropping below the freezing point in September, the ERT results of Krautblatter  
 312 et al. (2010) show refreezing from the rock face. Similar to the electrical resistivity, seis-  
 313 mic velocities are different for frozen and unfrozen material and sharply increase at the  
 314 freezing point (King et al., 1988; Leclaire et al., 1994; Kneisel et al., 2008). Laboratory  
 315 experiments including samples from Mt. Zugspitze show that this also holds for low-porosity

316 Wetterstein limestones representative for the study site (Draebing & Krautblatter, 2012).  
 317 The seasonal velocity changes can thus be explained by the annual heat wave causing  
 318 progressive thawing to depth starting in spring from the rock face, which will decrease  
 319 seismic velocities. The observed rapid decline of velocities is presumably enhanced by  
 320 water percolation from melt and precipitation. Once temperatures drop again below the  
 321 freezing point in fall, progressive refreezing from the rock face to depth will again increase  
 322 the velocities. The immediate response of the velocity to the temperature dropping be-  
 323 low and rising above the freezing point (fall and spring, respectively) appear plausible  
 324 in the light that centimeter-scale ground freezing is sufficient to result in significant sur-  
 325 face waves velocity changes (Steinmann et al., 2021). Finally, following the argumenta-  
 326 tion line from above, the long-term decrease in seismic velocities can be well explained  
 327 by permafrost degradation, i.e. the shrinkage of the perennially frozen rock volume due  
 328 to rising temperatures. This is also evident from borehole temperature logging beneath  
 329 the summit (Gallemann et al., 2017).

## 330 6 Conclusions

331 Using passive seismic data from Mt. Zugspitze, we find seasonal seismic velocity  
 332 changes as well as a velocity decrease over the observation period of 15 years. Compar-  
 333 ison of our results with meteorological data and a previous ERT study suggest that these  
 334 velocity changes are caused by seasonal freeze-thaw cycles and permafrost degradation,  
 335 respectively. Although originally deployed for earthquake monitoring, we were able to  
 336 exploit the seismic station for long-term permafrost monitoring yielding velocity change  
 337 values on more than 80% of all days in the 15-year observation period. This highlights  
 338 the cost and labour efficient potential of seismology for continuous permafrost monitor-  
 339 ing, compared to other methods where long-term monitoring is challenged by manual  
 340 data acquisition requiring regular field trips. Yet, the single station approach of this study  
 341 is limited in the spatial resolution. Future studies should therefore extend the instrumen-  
 342 tation in order to investigate permafrost dynamics with high spatio-temporal resolution.  
 343 In this context, the recently introduced distributed acoustic sensing systems, which al-  
 344 low wave propagation sensing on a meter scale along fiber-optic cables are promising for  
 345 detailed permafrost monitoring.

## 346 Acknowledgments

347 This study was financially supported by the Bayerisches Landesamt für Umwelt (LfU).  
 348 We gratefully acknowledge support from the staff of the Schneefernerhaus for hosting  
 349 the seismic station. Data of station BW.ZUGS is available through the EIDA node at  
 350 <http://erde.geophysik.uni-muenchen.de/fdsnws>, data of the meteorological station through  
 351 the DWD Climate Data Center (<https://cdc.dwd.de/portal/>, station ID 5792).

## 352 References

- 353 Becker, G., & Knapmeyer-Endrun, B. (2019). Crustal thickness from horizontal  
 354 component seismic noise auto- and cross-correlations for stations in central and  
 355 eastern Europe. *Geophysical Journal International*, *218*(1), 429–445.
- 356 Beniston, M., Farinotti, D., Stoffel, M., Andreassen, L. M., Coppola, E., Eckert, N.,  
 357 ... Vincent, C. (2018). The European mountain cryosphere: a review of its  
 358 current state, trends, and future challenges. *The Cryosphere*, *12*(2), 759–794.
- 359 Bennington, N., Ohlendorf, S., Thurber, C., & Haney, M. (2021). Spatiotemporal  
 360 analysis of seismic velocity changes at Okmok volcano, Alaska and implications  
 361 from deformation source modeling. *Earth and Planetary Science Letters*, *561*,  
 362 116809.
- 363 Bensen, G., Ritzwoller, M., Barmin, M., Levshin, A. L., Lin, F., Moschetti, M.,  
 364 ... Yang, Y. (2007). Processing seismic ambient noise data to obtain reli-

- 365 able broad-band surface wave dispersion measurements. *Geophysical Journal*  
 366 *International*, 169(3), 1239–1260.
- 367 Biskaborn, B. K., Smith, S. L., Noetzli, J., Matthes, H., Vieira, G., Streletskiy,  
 368 D. A., . . . Lantuit, H. (2019). Permafrost is warming at a global scale. *Nature*  
 369 *communications*, 10(1), 1–11.
- 370 Clarke, D., Zaccarelli, L., Shapiro, N., & Brenguier, F. (2011). Assessment of res-  
 371 olution and accuracy of the moving window cross spectral technique for mon-  
 372 itoring crustal temporal variations using ambient seismic noise. *Geophysical*  
 373 *Journal International*, 186(2), 867–882.
- 374 Davies, M. C., Hamza, O., & Harris, C. (2001). The effect of rise in mean annual  
 375 temperature on the stability of rock slopes containing ice-filled discontinuities.  
 376 *Permafrost and periglacial processes*, 12(1), 137–144.
- 377 Department of Earth and Environmental Sciences, Geophysical Observatory, LMU  
 378 Munich. (2001). *BayernNetz [Data set]*. International Federation of Digital  
 379 Seismograph Networks. doi: 10.7914/SN/BW
- 380 De Plaen, R. S., Lecocq, T., Caudron, C., Ferrazzini, V., & Francis, O. (2016).  
 381 Single-station monitoring of volcanoes using seismic ambient noise. *Geophysical*  
 382 *Research Letters*, 43(16), 8511–8518.
- 383 Draebing, D., & Krautblatter, M. (2012). P-wave velocity changes in freezing hard  
 384 low-porosity rocks: a laboratory-based time-average model. *The Cryosphere*,  
 385 6(5), 1163–1174.
- 386 Gallemann, T., Haas, U. H., Teipel, U., von Poschinger, A., Wagner, B., Mahr, M.,  
 387 & Bäse, F. (2017). Permafrost-Messstation am Zugspitzgipfel: Ergebnisse und  
 388 Modellberechnungen. *Geologica Bavarica*, 115, 1–77.
- 389 Gruber, S., & Haeberli, W. (2007). Permafrost in steep bedrock slopes and its  
 390 temperature-related destabilization following climate change. *Journal of Geo-*  
 391 *physical Research: Earth Surface*, 112(F2).
- 392 Gruber, S., Hoelzle, M., & Haeberli, W. (2004a). Permafrost thaw and destabiliza-  
 393 tion of alpine rock walls in the hot summer of 2003. *Geophysical research let-*  
 394 *ters*, 31(13).
- 395 Gruber, S., Hoelzle, M., & Haeberli, W. (2004b). Rock-wall temperatures in the  
 396 alps: modelling their topographic distribution and regional differences. *Per-*  
 397 *mafrost and Periglacial Processes*, 15(3), 299–307.
- 398 Gude, M., & Barsch, D. (2005). Assessment of geomorphic hazards in connection  
 399 with permafrost occurrence in the Zugspitze area (Bavarian Alps, Germany).  
 400 *Geomorphology*, 66(1-4), 85–93.
- 401 Guillemot, A., Helmstetter, A., Larose, É., Baillet, L., Garambois, S., Mayoraz, R.,  
 402 & Delaloye, R. (2020). Seismic monitoring in the Gugla rock glacier (Switzer-  
 403 land): ambient noise correlation, microseismicity and modelling. *Geophysical*  
 404 *Journal International*, 221(3), 1719–1735.
- 405 Haeberli, W., Hoelzle, M., Kääb, A., Keller, F., Vonder Mühl, D., & Wagner, S.  
 406 (1998). Ten years after drilling through the permafrost of the active rock  
 407 glacier Murtèl, Eastern Swiss Alps: answered questions and new perspectives.  
 408 In *Proceedings of the seventh international conference on permafrost* (pp. 403–  
 409 410).
- 410 Haeberli, W., Noetzli, J., Arenson, L., Delaloye, R., Gärtner-Roer, I., Gruber, S., . . .  
 411 Phillips, M. (2010). Mountain permafrost: development and challenges of a  
 412 young research field. *Journal of Glaciology*, 56(200), 1043–1058.
- 413 Harris, C., & Cook, J. D. (1986). The detection of high altitude permafrost in jotun-  
 414 heimen, norway using seismic refraction techniques: an assessment. *Arctic and*  
 415 *Alpine Research*, 18(1), 19–26.
- 416 Hauck, C. (2002). Frozen ground monitoring using dc resistivity tomography. *Geo-*  
 417 *physical research letters*, 29(21), 12–1.
- 418 Hauck, C. (2013). New concepts in geophysical surveying and data interpretation for  
 419 permafrost terrain. *Permafrost and Periglacial Processes*, 24(2), 131–137.

- 420 Hobiger, M., Wegler, U., Shiomi, K., & Nakahara, H. (2014). Single-station cross-  
 421 correlation analysis of ambient seismic noise: application to stations in the  
 422 surroundings of the 2008 Iwate-Miyagi Nairiku earthquake. *Geophysical Jour-  
 423 nal International*, *198*(1), 90–109.
- 424 Hoelzle, M., Mittaz, C., Etzelmüller, B., & Haerberli, W. (2001). Surface energy  
 425 fluxes and distribution models of permafrost in European mountain areas: an  
 426 overview of current developments. *Permafrost and Periglacial Processes*, *12*(1),  
 427 53–68.
- 428 Huggel, C., Allen, S., Deline, P., Fischer, L., Noetzi, J., & Ravanel, L. (2012). Ice  
 429 thawing, mountains falling—are alpine rock slope failures increasing? *Geology  
 430 Today*, *28*(3), 98–104.
- 431 James, S., Knox, H., Abbott, R., Panning, M., & Screaton, E. (2019). Insights  
 432 into permafrost and seasonal active-layer dynamics from ambient seismic noise  
 433 monitoring. *Journal of Geophysical Research: Earth Surface*, *124*(7), 1798–  
 434 1816.
- 435 James, S., Knox, H., Abbott, R., & Screaton, E. (2017). Improved moving window  
 436 cross-spectral analysis for resolving large temporal seismic velocity changes in  
 437 permafrost. *Geophysical Research Letters*, *44*(9), 4018–4026.
- 438 Jerz, H., & von Poschinger, A. (1995). Neuere Ergebnisse zum Bergsturz Eibsee-  
 439 Grainau. *Geologica Bavarica*(99), 383–398.
- 440 Jiang, C., & Denolle, M. A. (2020). Noisepy: A new high-performance python tool  
 441 for ambient-noise seismology. *Seismological Research Letters*, *91*(3), 1853–  
 442 1866.
- 443 Kane, D. L., Hinkel, K. M., Goering, D. J., Hinzman, L. D., & Outcalt, S. I. (2001).  
 444 Non-conductive heat transfer associated with frozen soils. *Global and Planetary  
 445 Change*, *29*(3-4), 275–292.
- 446 King, M. (1977). Acoustic velocities and electrical properties of frozen sandstones  
 447 and shales. *Canadian Journal of Earth Sciences*, *14*(5), 1004–1013.
- 448 King, M., Zimmerman, R., & Corwin, R. (1988). Seismic and electrical properties of  
 449 unconsolidated permafrost1. *Geophysical Prospecting*, *36*(4), 349–364.
- 450 Kneisel, C., Hauck, C., Fortier, R., & Moorman, B. (2008). Advances in geophysical  
 451 methods for permafrost investigations. *Permafrost and periglacial processes*,  
 452 *19*(2), 157–178.
- 453 Körner, H., & Ulrich, R. (1965). Geologische und felsmechanische Untersuchungen  
 454 für die Gipfelstation der Seilbahn Eibsee–Zugspitze. *Geologica Bavarica*(55),  
 455 404–421.
- 456 Krautblatter, M., Funk, D., & Günzel, F. K. (2013). Why permafrost rocks become  
 457 unstable: a rock–ice–mechanical model in time and space. *Earth Surface Pro-  
 458 cesses and Landforms*, *38*(8), 876–887.
- 459 Krautblatter, M., & Hauck, C. (2007). Electrical resistivity tomography monitoring  
 460 of permafrost in solid rock walls. *Journal of Geophysical Research: Earth Sur-  
 461 face*, *112*(F2).
- 462 Krautblatter, M., Verleysdonk, S., Flores-Orozco, A., & Kemna, A. (2010).  
 463 Temperature-calibrated imaging of seasonal changes in permafrost rock walls  
 464 by quantitative electrical resistivity tomography (Zugspitze, German/Austrian  
 465 Alps). *Journal of Geophysical Research: Earth Surface*, *115*(F2).
- 466 Leclaire, P., Cohen-Ténoudji, F., & Aguirre-Puente, J. (1994). Extension of Biot’s  
 467 theory of wave propagation to frozen porous media. *The Journal of the Acous-  
 468 tical Society of America*, *96*(6), 3753–3768.
- 469 Lecocq, T., Caudron, C., & Brenguier, F. (2014). Msnoise, a python package for  
 470 monitoring seismic velocity changes using ambient seismic noise. *Seismological  
 471 Research Letters*, *85*(3), 715–726.
- 472 Lomb, N. R. (1976). Least-squares frequency analysis of unequally spaced data. *As-  
 473 trophysics and space science*, *39*(2), 447–462.
- 474 Mao, S., Mordret, A., Campillo, M., Fang, H., & van der Hilst, R. D. (2020). On the

- 475 measurement of seismic traveltime changes in the time–frequency domain with  
 476 wavelet cross-spectrum analysis. *Geophysical Journal International*, 221(1),  
 477 550–568.
- 478 Mellor, M. (1973). Mechanical properties of rocks at low temperatures. In *2nd*  
 479 *international conference on permafrost, yakutsk, international permafrost asso-*  
 480 *ciation* (pp. 334–344).
- 481 Mollaret, C., Hilbich, C., Pellet, C., Flores-Orozco, A., Delaloye, R., & Hauck, C.  
 482 (2019). Mountain permafrost degradation documented through a network of  
 483 permanent electrical resistivity tomography sites. *The Cryosphere*, 13(10),  
 484 2557–2578.
- 485 Noetzli, J., & Gruber, S. (2009). Transient thermal effects in Alpine permafrost. *The*  
 486 *Cryosphere*, 3(1), 85–99.
- 487 Nötzli, J., Gruber, S., & Poschinger, A. v. (2010). Modellierung und Messung von  
 488 Permafrosttemperaturen im Gipfelgrat der Zugspitze, Deutschland. *Geograph-*  
 489 *ica Helvetica*, 65(2), 113–123.
- 490 Obermann, A., Planès, T., Larose, E., & Campillo, M. (2019). 4-D Imaging of  
 491 Subsurface Changes with Coda Waves: Numerical Studies of 3-D Combined  
 492 Sensitivity Kernels and Applications to the Mw 7.9, 2008 Wenchuan Earth-  
 493 quake. *Pure and Applied Geophysics*, 176(3), 1243–1254.
- 494 Pacheco, C., & Snieder, R. (2005). Time-lapse travel time change of multiply  
 495 scattered acoustic waves. *The Journal of the Acoustical Society of America*,  
 496 118(3), 1300–1310.
- 497 Pacheco, C., & Snieder, R. (2006). Time-lapse traveltime change of singly scattered  
 498 acoustic waves. *Geophysical Journal International*, 165(2), 485–500.
- 499 Phillips, M., Wolter, A., Lüthi, R., Amann, F., Kenner, R., & Bühler, Y. (2017).  
 500 Rock slope failure in a recently deglaciated permafrost rock wall at Piz Kesch  
 501 (Eastern Swiss Alps), February 2014. *Earth Surface Processes and Landforms*,  
 502 42(3), 426–438.
- 503 Pirulli, M. (2009). The Thurwieser rock avalanche (Italian Alps): Description and  
 504 dynamic analysis. *Engineering Geology*, 109(1-2), 80–92.
- 505 Ravel, L., Magnin, F., & Deline, P. (2017). Impacts of the 2003 and 2015 summer  
 506 heatwaves on permafrost-affected rock-walls in the Mont Blanc massif. *Science*  
 507 *of the Total Environment*, 609, 132–143.
- 508 Scandroglio, R., Draebing, D., Offer, M., & Krautblatter, M. (2021). 4D quanti-  
 509 fication of alpine permafrost degradation in steep rock walls using a laboratory-  
 510 calibrated electrical resistivity tomography approach. *Near Surface Geophysics*,  
 511 19(Near-Surface Geophysics for Geohazard Assessment), 241–260.
- 512 Scandroglio, R., Rehm, T., Limbrock, J. K., Kemna, A., Heinze, M., Pail, R., &  
 513 Krautblatter, M. (2021). *Decennial multi-approach monitoring of thermo-*  
 514 *hydro-mechanical processes, Kammstollen outdoor laboratory, Zugspitze*  
 515 *(Germany)*. EGU General Assembly 2021, online, 19–30 Apr 2021. doi:  
 516 <https://doi.org/10.5194/egusphere-egu21-13815>
- 517 Scargle, J. D. (1982). Studies in astronomical time series analysis. ii-statistical as-  
 518 pects of spectral analysis of unevenly spaced data. *The Astrophysical Journal*,  
 519 263, 835–853.
- 520 Schroeder, T., & Krautblatter, M. (2021). *A high-resolution multi-phase thermo-*  
 521 *geophysical permafrost rock model to verify long-term ERT monitoring at the*  
 522 *Zugspitze (German/Austrian Alps)*. EGU General Assembly 2021, online,  
 523 19–30 Apr 2021. doi: <https://doi.org/10.5194/egusphere-egu21-15231>
- 524 Sens-Schönfelder, C., & Wegler, U. (2006). Passive image interferometry and sea-  
 525 sonal variations of seismic velocities at Merapi Volcano, Indonesia. *Geophysical*  
 526 *research letters*, 33(21).
- 527 Steinmann, R., Hadziioannou, C., & Larose, E. (2021). Effect of centimetric freezing  
 528 of the near subsurface on Rayleigh and Love wave velocity in ambient seismic  
 529 noise correlations. *Geophysical Journal International*, 224(1), 626–636.

- 530 Timur, A. (1968). Velocity of compressional waves in porous media at permafrost  
531 temperatures. *Geophysics*, *33*(4), 584–595.
- 532 Ulrich, R., & King, L. (1993). Influence of mountain permafrost on construction in  
533 the Zugspitze mountains, Bavarian Alps, Germany. In *Proceedings of the Sixth*  
534 *Internatinnal Conference on Permafrost, Beijing* (pp. 625–630).
- 535 Walter, F., Amann, F., Kos, A., Kenner, R., Phillips, M., de Preux, A., . . . Yves  
536 (2020). Direct observations of a three million cubic meter rock-slope collapse  
537 with almost immediate initiation of ensuing debris flows. *Geomorphology*, *351*,  
538 106933.
- 539 Yates, A., Savage, M., Jolly, A., Caudron, C., & Hamling, I. (2019). Volcanic, coseis-  
540 mic, and seasonal changes detected at White Island (Whakaari) volcano, New  
541 Zealand, using seismic ambient noise. *Geophysical Research Letters*, *46*(1),  
542 99–108.
- 543 Zhang, T., Barry, R., Knowles, K., Heginbottom, J., & Brown, J. (2008). Statistics  
544 and characteristics of permafrost and ground-ice distribution in the Northern  
545 Hemisphere. *Polar Geography*, *31*(1-2), 47–68.